Available online at www.sciencedirect.com
ScienceDirect
J. Chem. Thermodynamics 40 (2008) 980–990
JCT
www.elsevier.com/locate/jct

Solubility measurements of the uranyl oxide hydrate phases metaschoepite, compreignacite, Na–compreignacite, becquerelite, and clarkeite

Drew Gorman-Lewis [a,*], Jeremy B. Fein [a], Peter C. Burns [a,b], Jennifer E.S. Szymanowski [a], Jenalee Converse [a]

[a] University of Notre Dame, Department of Civil Engineering and Geological Sciences, 156 Fitzpatrick Hall, Notre Dame, IN 46556, United States
[b] Chemistry Division, Argonne National Laboratory, Argonne, IL 60439, United States

Received 12 November 2007; received in revised form 28 January 2008; accepted 12 February 2008
Available online 19 February 2008

Abstract

The mobility of uranium under oxidizing conditions can only be modeled if the thermodynamic stabilities of the secondary uranyl minerals are known. Toward this end, we synthesized metaschoepite ($UO_3(H_2O)_2$), becquerelite ($Ca(UO_2)_6O_4(OH)_6(H_2O)_8$), compreignacite ($K_2(UO_2)_6O_4(OH)_6(H_2O)_7$), sodium compreignacite ($Na_2(UO_2)_6O_4(OH)_6(H_2O)_7$), and clarkeite ($Na(UO_2)O(OH)$) and performed solubility measurements from both undersaturation and supersaturation under controlled-pH conditions. The solubility measurements rigorously constrain the values of the solubility products for these synthetic phases, and consequently the standard-state Gibbs free energies of formation of the phases. The calculated lg solubility product values ($\lg K_{sp}$), with associated 1σ uncertainties, for metaschoepite, becquerelite, compreignacite, sodium compreignacite, and clarkeite are (5.6 −0.2/+0.1), (40.5 −1.4/+0.2), (35.8 −0.5/+0.3), (39.4 −1.1/+0.7), and (9.4 −0.9/+0.6), respectively. The standard-state Gibbs free energies of formation, with their 2σ uncertainties, for these same phases are (-1632.2 ± 7.4) kJ · mol^{-1}, (-10305.6 ± 26.5) kJ · mol^{-1}, (-10107.3 ± 21.8) kJ · mol^{-1}, (-10045.6 ± 24.5) kJ · mol^{-1}, and (-1635.1 ± 23.4) kJ · mol^{-1}, respectively. Combining our data with previously measured standard-state enthalpies of formation for metaschoepite, becquerelite, sodium compreignacite, and clarkeite yields calculated standard-state entropies of formation, with associated 2σ uncertainties, of (-532.5 ± 8.1) J · mol^{-1} · K^{-1}, (-3634.5 ± 29.7) J · mol^{-1} · K^{-1}, (-2987.6 ± 28.5) J · mol^{-1} · K^{-1}, and (-300.5 ± 23.9) J · mol^{-1} · K^{-1}, respectively. The measurements and associated calculated thermodynamic properties from this study not only describe the stability and solubility at $T = 298$ K, but also can be used in predictions of uranium mobility through extrapolation of these properties to temperatures and pressures of geologic and environmental interest.

Keywords: Solubility; Uranyl oxide hydrate; Gibbs free energy of formation; Uranium

1. Introduction

The mobility of uranium in oxidizing environments can be significantly impacted by the stability and solubility of uranyl (U^{6+}) minerals. Uranyl mineral assemblages tend to be highly complex, and multiple phases can be present in intimate intergrowths. These minerals form where uraninite is oxidized, and the identity, abundance, and order of appearance of the important secondary phases depend upon the local geochemistry. Uranyl oxide hydrates can be the first alteration phases to form [1].

The uranyl oxide hydrates are a complex group of minerals consisting of more than 20 species [1]. The structural unit in each of these minerals consists of infinite two-dimensional sheets of edge and vertex sharing uranyl polyhedra [2]. The interlayer regions of these structures contain H_2O groups, and in most cases mono or divalent cations

* Corresponding author. Present address: University of Washington, Department of Earth and Space Sciences, Johnson Hall Box 351310, Seattle, WA 98195, United States. Tel.: +1 206 543 3541.
E-mail address: dgormanl@u.washington.edu (D. Gorman-Lewis).

0021-9614/$ - see front matter © 2008 Elsevier Ltd. All rights reserved.
doi:10.1016/j.jct.2008.02.006

that provide for electro-neutrality and linkages between the sheets. The topological aspects of the sheets of polyhedra are diverse, but multiple phases are also known that contain topologically identical sheets. The details of the interlayer constituents and their bonding to the sheets of uranyl polyhedra impact the stabilities of these minerals [3,4].

Where uraninite is altered under moist, oxidizing conditions, uranyl oxide hydrates are typically the first phases to form [1,5,6]. These minerals often form where anthropogenic nuclear materials interact with the environment. Considerable research has focused on the formation of uranyl phases where spent nuclear fuel is altered in a moist, oxidizing environment, similar to conditions expected in the proposed repository at Yucca Mountain, Nevada. Finch *et al.* [7] examined the alteration phases that formed on commercial spent nuclear fuel over several years of alteration in a hydrologically unsaturated environment at $T = 363$ K and found that uranyl oxide hydrates formed first and were abundant. Wronkiewicz *et al.* [8,9] conducted similar unsaturated tests at $T = 363$ K using non-irradiated UO_2 for 10 years, and found a similar dominance of uranyl oxide hydrate phases. Studies of natural analogues for a geological repository in the unsaturated region have also demonstrated the importance of uranyl oxide hydrate minerals [10,11].

Burns *et al.* [12] proposed that uranyl oxide hydrates that form in a geological repository during the alteration of spent nuclear fuel could incorporate various radionuclides into their structures, thereby potentially reducing their mobility. Owing to its long half-life and potential mobility in groundwater, ^{237}Np is particularly important for assessing the long-term performance of a geological repository in the unsaturated zone. Experiments by Burns *et al.* [13], Douglas *et al.* [14,15], and Klingensmith *et al.* [16] have all provided evidence for incorporation of Np^{5+} into uranyl phases, including uranyl oxide hydrates, indicating that the solubilities of these minerals under repository conditions could impact Np mobility.

Despite the potential importance of uranyl oxide hydrate phases in controlling uranium mobility under oxidizing conditions, reliable thermodynamic data are lacking for most of these minerals [17]. In order to predict the stability and solubility of uranyl oxide hydrate phases as a function of solution composition (pH, ionic strength, *etc.*), the standard-state Gibbs free energy of formation for each phase of interest must be known. Reliable measurements of the Gibbs free energy of formation of a mineral phase can be derived from solubility studies only when the following conditions are met: (1) the mineral of interest is demonstrated to be stable under the experimental conditions, (2) a true and demonstrable equilibrium state is attained during the experiments, and (3) the pH and aqueous metal concentrations present under the equilibrium conditions are measured. Thorough solid phase characterization both before and after the solubility experiment, performance of reversibility experiments, and measurements of all dissolved cations are all crucial in order to yield reliable thermodynamic parameters from the experimental results.

Most previous measurements of metaschoepite, becquerelite, compreignacite, and clarkeite have lacked one or more aspects for rigorous solubility determinations [17]. Previous studies of uranyl oxide hydrates are summarized by Gorman-Lewis *et al.* [17], and in general there is considerable uncertainty associated with the solubility product for many of these phases, perhaps caused by effects of variations in solid phase crystallinity. However, another source of uncertainties may be that few uranyl oxide hydrate solubility studies have been conducted from both supersaturated and undersaturated conditions, and post-experimental residue analyses have also varied greatly or have been absent. In the present study, we report solubility results for metaschoepite ($UO_3(H_2O)_2$), becquerelite ($Ca(UO_2)_6O_4(OH)_6(H_2O)_8$), compreignacite ($K_2(UO_2)_6O_4(OH)_6(H_2O)_7$), sodium compreignacite ($Na_2(UO_2)_6O_4(OH)_6(H_2O)_7$), and clarkeite ($Na(UO_2)O(OH)$). We use the experimental results to rigorously constrain K_{sp}values for each phase, enabling calculation of the standard state Gibbs free energy of formation for each phase studied.

2. Experimental materials and methods

2.1. Syntheses

All synthetic methods were derived from procedures described in [18]. ACS grade reagents and 18 MΩ H_2O were used in all syntheses. Teflon liners in the Parr bombs were run through numerous heated cycles with H_2O prior to use in order to minimize release of HF into the synthesis solutions. UO_3 can absorb H_2O from the air so to ensure a consistent starting material amorphous UO_3 was prepared by dissolving UO_3 in ~6 M HNO_3 and heating the mixture to dryness until all gases had evolved and the solid was a uniform orange color. $UO_2(CH_3COO)_2(H_2O)_2$ was prepared by gently heating (just below boiling) ~0.5 g of freshly prepared UO_3 with ~600 cm^3 glacial acetic acid until dryness. Metaschoepite was synthesized by adding amorphous UO_3 with 5 cm^3 of H_2O to a Teflon lined Parr bomb and heating the mixture at $T = 348$ K for 24 h. Becquerelite was synthesized by combining 0.313 g $UO_2(CH_3COO)_2(H_2O)_2$, 0.05 g $CaCO_3$, and 4 cm^3 H_2O in a Teflon lined Parr bomb and heating the mixture at $T = 433$ K for 50 h. Compreignacite was synthesized by adding 0.21 g $UO_2(CH_3COO)_2(H_2O)_2$, 0.03 g K_2CO_3, and 5 cm^3 H_2O. The pH of the mixture was adjusted to ~5 and heated at $T = 373$ K for 24 h in a Teflon lined Parr bomb. The Na–compreignacite synthesis was identical to compreignacite except 0.31 g of Na_2CO_3 was substituted for the K_2CO_3. Clarkeite was synthesized by adding 0.0843 g $UO_2(CH_3COO)_2(H_2O)_2$, 0.17 g Na_2CO_3, and 10 cm^3 H_2O to a Teflon lined Parr bomb, and heating the mixture at $T = 493$ K for 14 d. After synthesis, all batches of minerals were rinsed with boiling H_2O and air dried prior to characterization.

2.2. Characterization

X-ray powder diffraction patterns were collected for each batch of synthesized powder by finely grinding ~5 mg of powder and depositing the paste onto a zero-background orientated quartz slide. Diffraction patterns were collected using a Bruker D8 Discovery diffractometer equipped with Cu Kα radiation and a solid-state detector. All powder diffraction patterns exhibited sharp profiles and no extraneous peaks, and they confirmed the presence of synthesized mineral as the only crystalline phase (patterns shown in Supplementary materials figure S1). FT-IR analyses were performed using an IlluminatIR FT-IR microspectrometer with a diamond total attenuated reflectance (ATR) objective in an open atmosphere, background spectra taken prior to measurement, over a frequency range of (400 to 4000) cm^{-1} using ~(5 to 10) mg of powder placed on a glass slide. The IR spectra were in good agreement with previously published spectra [19]. Thermogravimetric (TGA) analyses were carried out by heating the powder to $T = 973$ K at 10 K min^{-1} under flowing nitrogen at 14 $cm^3 \cdot min^{-1}$. Water content was calculated from the weight loss (results shown in Supplementary materials table S1). Chemical analyses were performed by dissolving ~(5 to 10) mg of powder in ~50 cm^3 of 2 M HCl and analyzing for total aqueous uranium and the cation of interest in each oxide hydrate phase, using inductively coupled plasma-optical emission spectrometry (ICP-OES) with an analytical uncertainty of 3.5% (results shown in Supplementary materials table S1).

2.3. Solubility experiments

All solubility measurements were conducted as batch experiments using Teflon reaction vessels. An Orion combination pH electrode that was calibrated daily with 4 NIST standards (pH 2, 4, 7, and 10) was used for pH measurements. Although the ionic strength of the buffers was not perfectly matched to the ionic strength of the experiments, the additional error associated with pH measurements as a result of the difference in ionic strength and liquid-junction error is likely much smaller than experimental error which dominates the stated uncertainties for the calculated thermodynamic parameters [20]. In order to decrease the time necessary to reach equilibrium, we started the experiments in solutions containing dissolved U and the appropriate cation for each solid phase present. The initial experimental solutions were prepared using aliquots of stock solutions, prepared by adding the appropriate nitrate salt to 18 MΩ H_2O, and diluting to the desired concentrations. Approximately, 350 mg of the synthesized phase of interest was added to either ~7 cm^3 (small volume experiments) or ~125 cm^3 (large volume experiments) of the prepared starting solution. The pH of the batch experiments was adjusted using minute quantities of concentrated HNO_3 and/or NaOH or KOH. The pH was monitored daily and adjusted as needed throughout each experiment. The pH descriptor for each experiment is the average of the pH of the plateau data points; however, the actual pH measurement for each data point was used in calculations. Reaction vessels were sealed and agitated slowly end over end. Aliquots of the experimental solution were taken extracted at various times, filtered through 0.1 μm nylon filters, and diluted and acidified for ICP-OES analysis to determine dissolved concentrations of U, Ca, Na, and K concentrations with an analytical uncertainty of 3.5%. In order to verify the composition of the mineral residue after 7 d of reaction and at the end of each experiment, ~10 mg of residue was collected for XRD and FT-IR analyses.

Initial experimental results indicated that in (1 to 16) mM $NaNO_3$, pH (3.5 to 5.5) solutions clarkeite transforms entirely to metaschoepite. Previous dissolution studies of metaschoepite and soddyite run in electrolyte concentrations of 10 mM $NaNO_3$ at pH 6 found the ingrowth of a clarkeite-like phase [21,22]. Therefore, in order to ensure clarkeite stability, we ran the clarkeite experiments in 0.1 M $NaNO_3$, increasing the Na^+ concentration by an order of magnitude over previous experiments that found conditions under which clarkeite is stable. The post-experimental residue analysis revealed a co-existence of clarkeite and metaschoepite in these systems. The co-existence of two phases (clarkeite and metaschoepite) in the experimental systems is consistent with the Gibbs phase rule for two-component systems such as these. If both phases are stable under the experimental conditions and we measure all dissolved element concentrations, then the experimental measurements rigorously constrain the value of the solubility products for each phase present. Control experiments in a previous study under similar conditions, performed without mineral phases present, indicated that the loss of U to adsorption or precipitation reactions under the experimental conditions was negligible [23].

3. Results and discussion

3.1. Solubility experiments

Metaschoepite reaches steady-state, as defined by an aqueous U concentration plateau, from undersaturated conditions within 2 d for experiments from pH (3.6 to 4.3) (figure 1). Two additional experiments starting from supersaturated conditions at pH (3.6 and 3.8) attained steady-state within 3 d. All post-experimental residue analyses revealed that metaschoepite was the only phase present. The observed concentrations of dissolved U under steady-state conditions decreased with increasing pH over the pH range studied.

Becquerelite experiments at pH (3.2 and 4.4) reached steady-state conditions within 3 d (figure 2). Supersaturated experiments, conducted at pH (5.0 and 5.2), required (9 to 13) d to reach steady-state conditions. All experiments exhibited non-stoichiometric dissolution with an excess of Ca in solution. The XRD and FTIR of the experimental residues suggested that becquerelite was the only phase

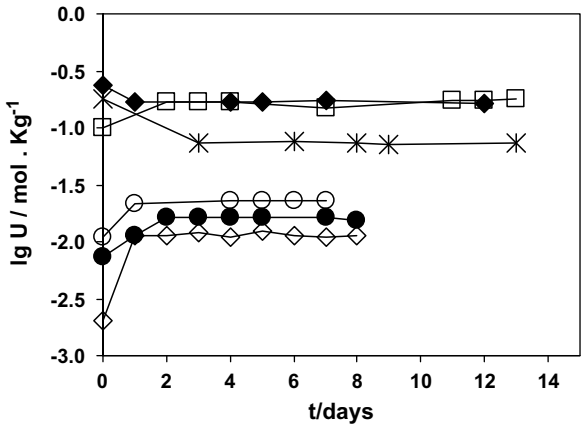

FIGURE 1. Plot of experimental measurements of solubility U as lg(U/mol · kg^{-1}) against time for metaschoepite with experiments at pH 3.6 (open squares and closed diamonds), pH 3.8 (stars), pH 4.1, (open circles), pH 4.2 (closed circles), and pH 4.3 (open diamonds).

present; however, the XRD results did reveal a decrease in the crystallinity of the phase. We attribute the decrease in crystallinity of the mineral phase to preferential leaching of Ca out of the phase and concurrent proton incorporation to maintain charge balance. A previous study on the dissolution of becquerelite also noted a leaching of Ca out of the mineral phases and reduction in the crystallinity [4]. As is the case for metaschoepite, the solubility of becquerelite decreases markedly with increasing pH over the pH range of these experiments.

Figure 3 illustrates the compreignacite solubility data for experiments from pH (4.3 to 4.6). Reaching steady-state conditions from undersaturated conditions took (3 to 4) d, while achieving a steady state from supersaturated conditions took approximately (7 to 14) d. Similar to our results for becquerelite, we observed non-stoichiometric dissolution, with an excess of K in solution. Post-experimental analyses of mineral residues revealed compreignacite as the only phase present; however, as was the case in the becquerelite experiments, there was a significant loss in the crystallinity of the mineral phase during the experiments. Burns [24] systematically described uranyl crystal chemistry by the topological arrangement of anions within the sheets of polyhedra that make up uranyl minerals. Based on this classification, becquerelite, compreignacite, and sodium compreignacite share the protasite sheet structure, and have identical anion distributions, making preferential cation leaching possible.

Sodium compreignacite solubility results from pH (4.0 to 5.3), shown in figure 4, illustrate that from 2 d to approximately 20 d are necessary for steady-state conditions to be attained under the experimental conditions. Similar to compreignacite and becquerelite, the observed dissolution was non-stoichiometric, with an excess of Na present in solution. Post-experimental residue analyses

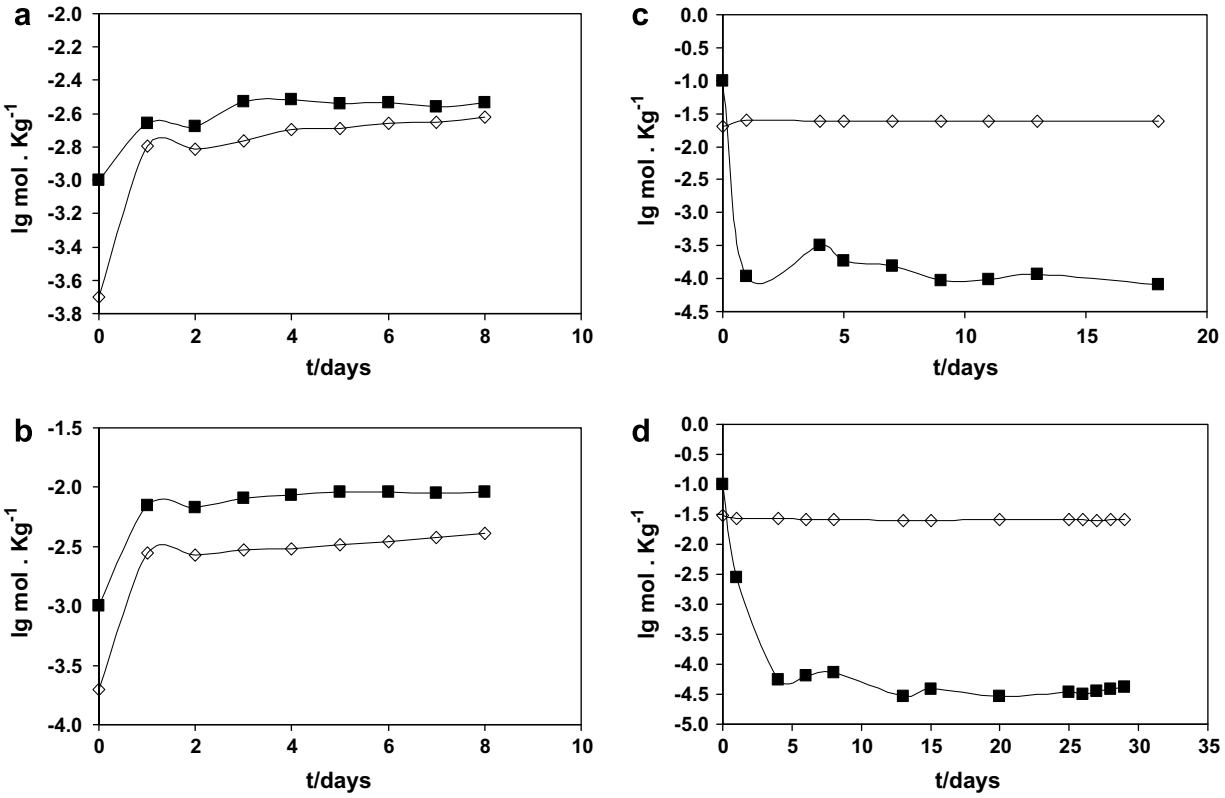

FIGURE 2. Plot of experimental measurements of the solubility U as lg(U/mol · kg^{-1}) against time for becquerelite (U – filled squares and Ca – open diamonds) for experiments at pH 4.4 (a), 3.2 (b), 5. 0 (c), 5.2 (d).

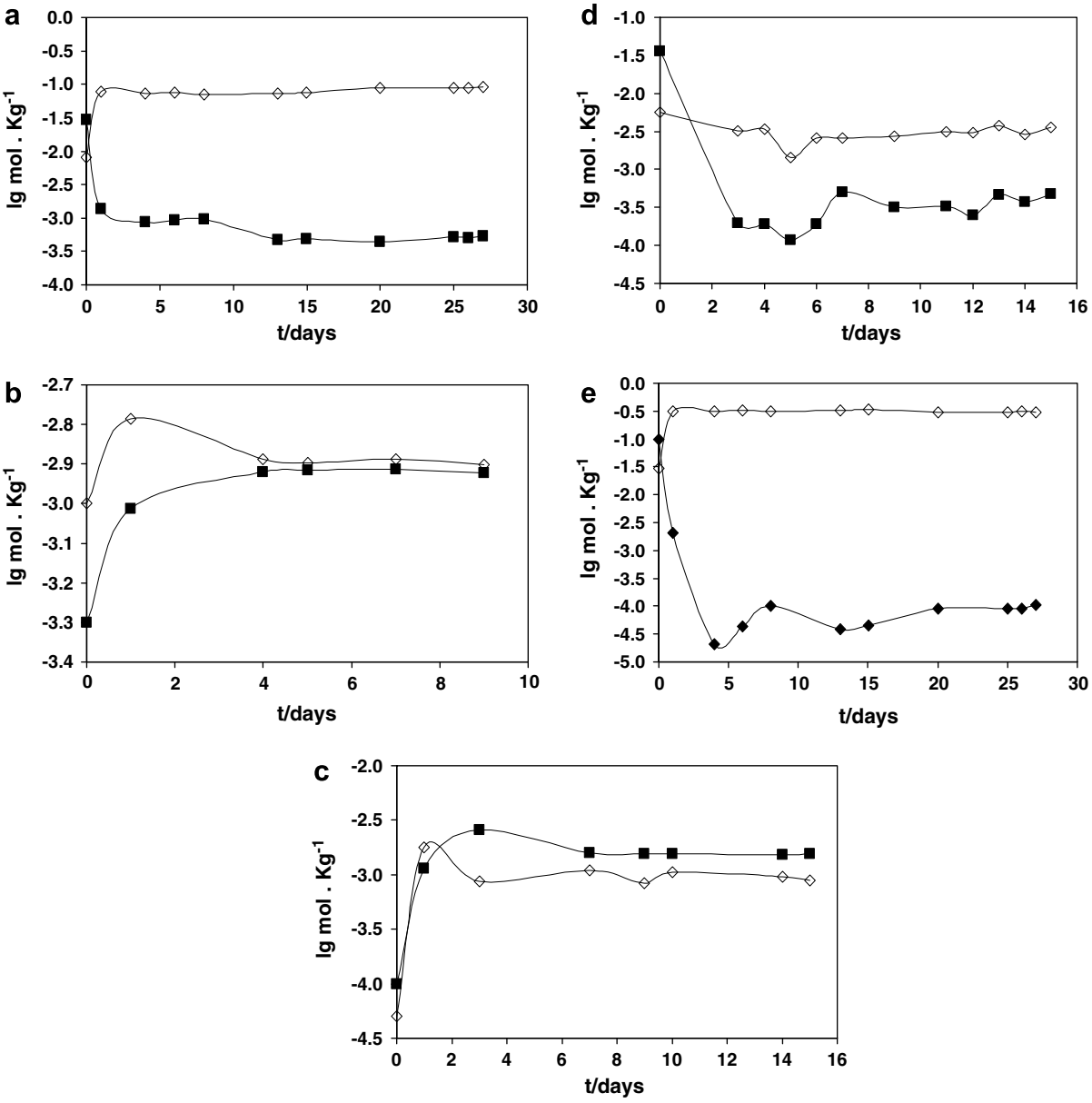

FIGURE 3. Plot of experimental measurements of the solubility U as lg(U/mol · kg^{-1}) against time for compreignacite (U – filled squares and K – open diamonds) for experiments at pH 4.3 (a), 4.4 (b), 4.4 (c), 4.5 (d), 4.6 (e).

revealed sodium compreignacite as the only phase present, with some loss in crystallinity.

The preferential leaching of the interlayer cations (Ca^{2+}, K^{+}, and Na^{+}) in becquerelite, compreignacite, and sodium compreignacite may suggest a steady state in the solid between the outer leached layer of the mineral and the bulk material. Our solubility results depict steady states between the aqueous solution and the outer leach layer of the minerals. A steady state between the aqueous solution and the inner bulk material may be implied if a steady state between the outer leach layer and the inner bulk material is indeed achieved. Additional experiments such as high temperature oxide melt calorimetry on well-characterized leached layer phases could provide further insight into the preferential leaching of these phases.

All clarkeite solubility experiments, with the exception of the pH (4.2 and 4.3) experiments, exhibited an initial decrease in dissolved U concentration followed by a subsequent increase and attainment of a steady-state plateau (figure 5). The initial decrease in U concentration is likely due to the precipitation of metaschoepite, and this phase was found to be present in all experimental residues along with clarkeite. In preliminary experiments, conducted using less than 0.1 M $NaNO_3$, we found that clarkeite was not stable and that the mineral was converted entirely to metaschoepite. Giammar and Hering also found the coexistence of metaschoepite and a clarkeite-like phase in systems investigating the solubility of metaschoepite in the presence of 0.01 M $NaNO_3$ [21]. In our clarkeite experiments, steady-state conditions were attained in between

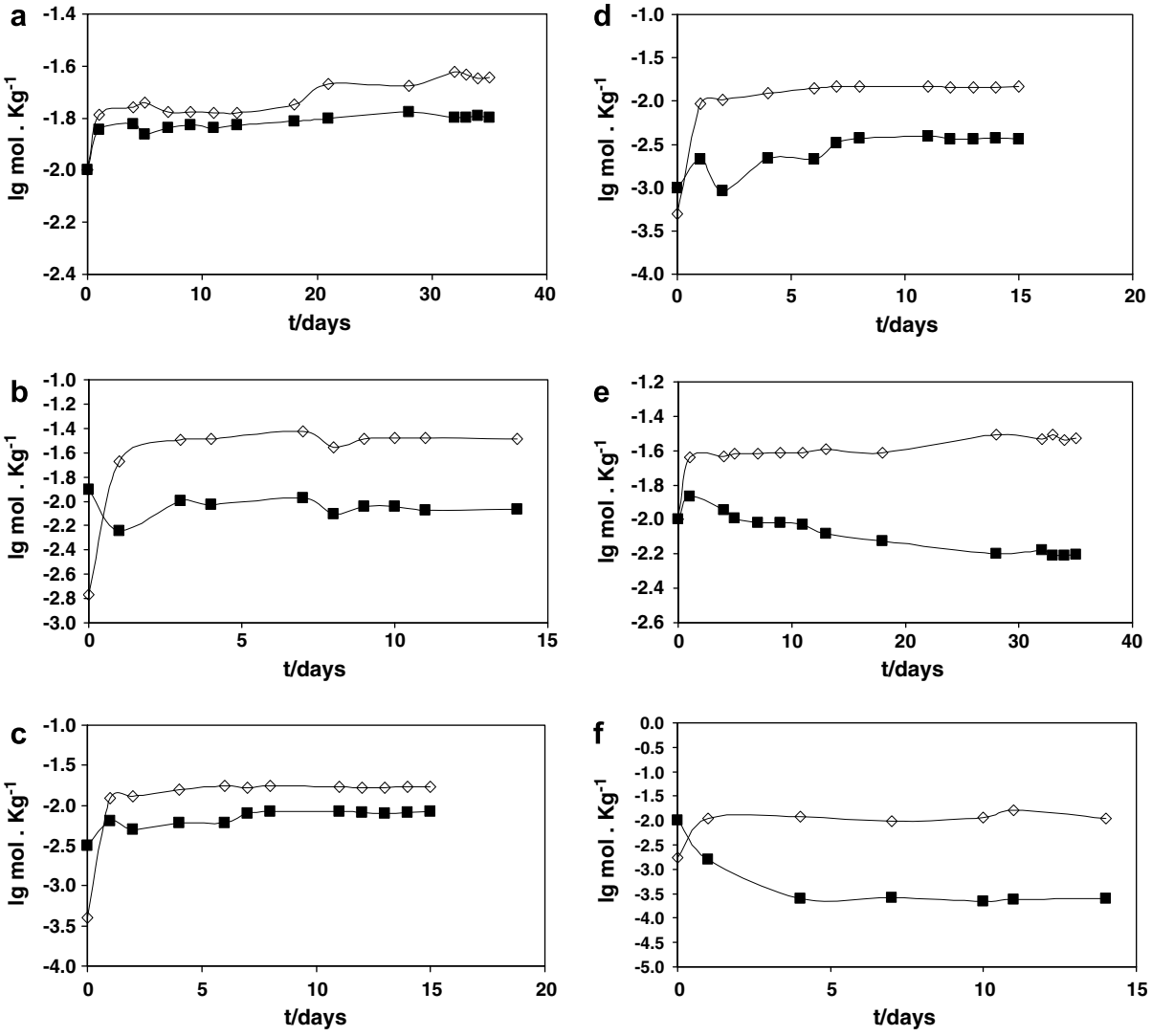

FIGURE 4. Plot of experimental measurements of the solubility U as $\lg(\mathrm{U/mol \cdot kg^{-1}})$ against time for Na–compreignacite (U – filled squares and Na – open diamonds) for experiments at pH 4.0 (a), 4.1 (b), 4.1 (c), 4.3 (d & e), 5.3 (f).

3 d and approximately 40 d, and in general, the steady-state U concentration decreased with increasing pH, although there is not a large difference between the U concentrations in the pH ~5.7 and the pH ~6.4 experiments.

3.2. Solubility product calculations

We based our solubility calculations on the dissolution reactions listed in table 1. For each solubility measurement on the equilibrium concentration plateau (data points compiled in Supplementary materials tables S2 to S6), we calculated the ionic strength of the solution from the concentration of U, Na, K, and the pH measurement for each sample, and the known amount of acid added for pH adjustments to take into account the concentration of NO_3^- in each system for ionic strength calculations. We used the extended Debye–Hückel equation to calculate the activity coefficients, γ_i, for each experimental condition:

$$\log \gamma_i = \frac{-Az_i^2\sqrt{I}}{1 + aB\sqrt{I}} + bI, \quad (1)$$

where I and z_i represent the ionic strength and ionic charge, respectively; A and B are constants with values of 0.5105 and 0.3285 [25], respectively, and a and b are values for $RbNO_3$ from Helgeson *et al.* [25] of 5.22 and 0.062, respectively. Parameters a and b take unique values for a particular electrolyte. Because in all of the experiments except for the clarkeite experiments, we did not buffer ionic strength with such an electrolyte, and because values of a and b have not been determined for uranyl-dominated systems; $RbNO_3$ was chosen as the most reasonable approximation for these experimental solutions, based on cation size, of those for which extended Debye–Hückel parameters are calculated [25]. For internal consistency, we used the $RbNO_3$ a and b values for the clarkeite experiments as well. The standard-states employed in this study for solid phases and for H_2O are the pure mineral or fluid, respectively, at

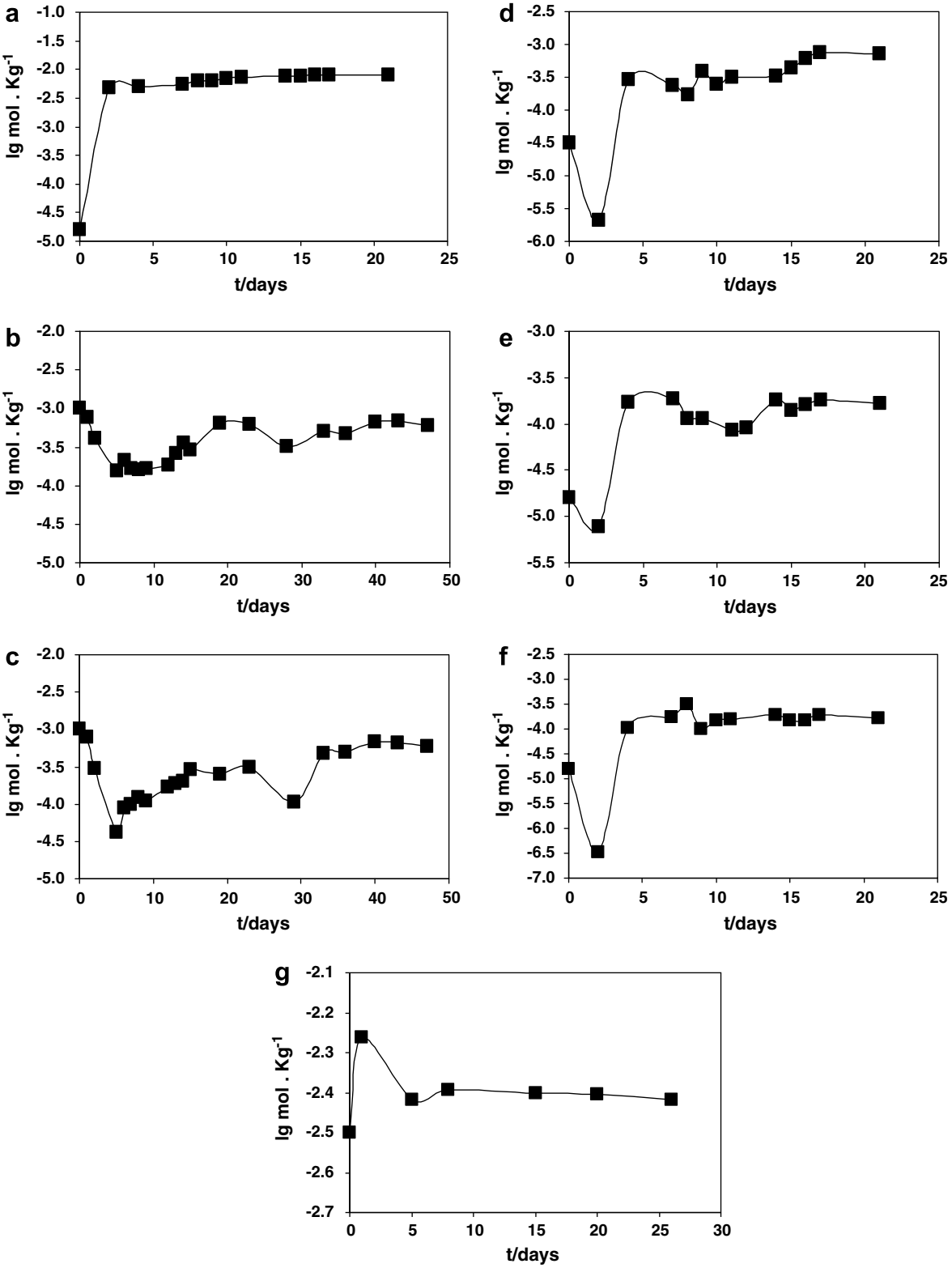

FIGURE 5. Plot of experimental measurements of the solubility U as $\lg(U/\text{mol} \cdot \text{kg}^{-1})$ against time for clarkeite (U) in 0.1 M $NaNO_3$ for experiments at pH 4.2 (a), 4.7 (b), 4.7 (c), 4.8 (d), 5.7 (e), 6.4 (f), 4.3 (g).

the temperature and pressure of the experiments. The standard-state for aqueous species is defined as a hypothetical one molal solution whose behavior is that of infinite H_2O dilution. Molal activity coefficients of neutral aqueous species are assumed to be unity. Using these standard-states, and assuming that the solid phase is pure and that the activity of water can be represented by the mole fraction of water (N_{H2O}) under the experimental conditions, the sol-

TABLE 1

Mineral phase	Dissolution reactions	Mass action equations	$\lg K_{sp} \pm 1\sigma$ ($I = 0$)
Metaschoepite	$2H^+ + UO_3(H_2O)_2 = UO_2^{2+} + 3H_2O$	$K_{sp} = N_{H_2O}^3 \cdot a_{UO_2^{2+}} \cdot a_{H^+}^{-2}$	5.6 (−0.2/ +0.1)
Becquerelite	$Ca(UO_2)_6O_4(OH)_6(H_2O)_8 + 14H^+ = Ca^{2+} + 6UO_2^{2+} + 18H_2O$	$K_{sp} = N_{H_2O}^{18} \cdot a_{Ca^{2+}} \cdot a_{UO_2^{2+}}^6 \cdot a_{H^+}^{-14}$	40.5 (−1.4/ +0.2)
Compreignacite	$K_2(UO_2)_6O_4(OH)_6(H_2O)_7 + 14H_+ = 2K^+ + 6UO_2^{2+} + 17H_2O$	$K_{sp} = N_{H_2O}^{17} \cdot a_{K^+}^2 \cdot a_{UO_2^{2+}}^6 \cdot a_{H^+}^{-14}$	35.8 (−0.5/ + 0.3)
Sodium compreignacite	$Na_2(UO_2)_6O_4(OH)_6(H_2O)_7 + 14H^+ = 2Na^+ + 6UO_2^{2+} + 17H_2O$	$K_{sp} = N_{H_2O}^{17} \cdot a_{Na^+}^2 \cdot a_{UO_2^{2+}}^6 \cdot a_{H^+}^{-14}$	39.4 (−1.1/ +0.7)
Clarkeite	$3H^+ + Na(UO_2)O(OH) = Na^+ + UO_2^{2+} + 2H_2O$	$K_{sp} = N_{H_2O}^2 \cdot a_{Na^+} \cdot a_{UO_2^{2+}} \cdot a_{H^+}^{-3}$	9.4 (−0.9/ +0.6)

ubility product for each steady-state data point, listed in Supplementary materials tables S2 to S6, was calculated based on the mass action equations listed in table 1. The assumption that the activity of water is equal to N_{H_2O} has been shown to be reasonable for solutions with a total dissolved solids concentration less than or equal to that of seawater [26]. When calculating the solubility product, the aqueous complexation reactions listed in table 2 were taken into consideration in order to calculate the activity of the aqueous uranyl cation under each experimental condition from our measurement of total aqueous uranium concentration. The errors associated with the stability constants in table 2 (errors not shown) were not propagated through the K_{sp} calculations; however, the uncertainty in the experimental measurements likely dominates the errors associated with the K_{sp} values. Uncertainty associated with the aqueous stability constants in table 2 would likely have a negligible effect on our calculated K_{sp} values. The calculated solubility products, averaged for all of the equilibrium measurements, with their 1σ uncertainties for each phase are listed in table 1.

TABLE 2
Aqueous complexation reactions

	$\lg K$ ($I = 0$)	Reference
$UO_2^{2+} + H_2O = UO_2OH^+ + H^+$	−5.25	[38]
$UO_2^{2+} + 2H_2O = UO_2(OH)_2^\circ + 2H^+$	−12.15	[38]
$UO_2^{2+} + 3H_2O = UO_2(OH)_3^- + 3H^+$	−20.25	[38]
$UO_2^{2+} + 4H_2O = UO_2(OH)_4^{2-} + 4H^+$	−32.4	[38]
$2UO_2^{2+} + H_2O = (UO_2)_2OH^{3+} + H^+$	−2.70	[38]
$2UO_2^{2+} + 2H_2O = (UO_2)_2(OH)_2^{2+} + 2H^+$	−5.62	[38]
$3UO_2^{2+} + 5H_2O = (UO_2)_3(OH)_5^+ + 5H^+$	−15.55	[38]
$3UO_2^{2+} + 7H_2O = (UO_2)_3(OH)_7^- + 7H^+$	−32.20	[38]
$4UO_2^{2+} + 7H_2O = (UO_2)_4(OH)_7^+ + 7H^+$	−21.90	[38]
$UO_2^{2+} + CO_3^{2-} = UO_2CO_3$	9.94	[38]
$UO_2^{2+} + 2CO_3^{2-} = UO_2(CO_3)_2^{2-}$	16.61	[38]
$UO_2^{2+} + 3CO_3^{2-} = UO_2(CO_3)_3^{4-}$	21.84	[38]
$3UO_2^{2+} + 6CO_3^{2-} = (UO_2)_3(CO_3)_6^{6-}$	54.00	[38]
$2UO_2^{2+} + CO_3^{2-} + 3H_2O = (UO_2)_2CO_3(OH)_3^- + 3H^+$	−0.86	[38]
$3UO_2^{2+} + CO_3^{2-} + 3H_2O = (UO_2)_3O(OH)_2(HCO_3)^+ + 3H^+$	0.65	[38]
$11UO_2^{2+} + 6CO_3^{2-} + 12H_2O = (UO_2)_{11}(CO_3)_6(OH)_{12}^{2-} + 12H^+$	36.40	[38]
$Na^+ + CO_3^{2-} = NaCO_3^-$	−1.27	[39]
$Na^+ + CO_3^{2-} + H^+ = NaHCO_3^\circ$	−10.03	[39]
$Na^+ + OH^- = NaOH$	−14.18	[39]
$Na^+ + CO_3^{2-} + H^+ = NaHCO_3^\circ$	−10.03	[39]
$Ca^{2+} + CO_3^{2-} = CaCO_3^\circ$	3.224	[39]
$Ca^{2+} + CO_3^{2-} + H^+ = CaHCO_3^+$	11.435	[39]
$Ca^{2+} + OH^- = CaOH^+$	−12.78	[39]
$K^+ + OH^- = KOH^\circ$	−14.46	[39]

Previous measurements of metaschoepite solubility have produced $\lg K_{sp}$ values from (4.68) to (6.23) [27,21,28–31]. The only previous study to meet all the criteria for rigorous solubility studies as outlined above and with extrapolation of the K_{sp} value to zero ionic strength produced the lowest K_{sp} value (4.68) of the previous results [31]. Meinrath *et al.* [31] performed these experiments under an atmosphere of 0.3% CO_2 which may have affected the solubility through aqueous uranyl-carbonate complexation. Our K_{sp} for metaschoepite is within the range of previously published values; however, this study is the first to report results from reversibility experiments, to characterize the final run products, and to extrapolate calculated K_{sp} values to zero ionic strength.

There have also been numerous measurements of the solubility of synthetic becquerelite, producing $\lg K_{sp}$ values from (41.89) to (43.70) [32–34]; however, none of these studies constrained K_{sp} values by conducting experiments that started from supersaturated conditions. Casas *et al.* [35] measured the solubility of becquerelite using a natural sample and calculated a $\lg K_{sp}$ value of (29). These authors did collect data from both supersaturation and undersaturation; however, their post-experimental analysis revealed the formation of soddyite in the system, likely resulting from silica impurities found in the natural sample. Their much lower K_{sp} value than that found for synthetic becquerelite may result from the precipitation of soddyite in the system as well as the higher crystallinity of a natural sample relative to a synthetically produced phase. The calculated $\lg K_{sp}$ value for becquerelite from this study (40.5 (−1.4/+0.2)) is lower than that of previous measurements for synthetic becquerelite, however because our experiments were reversed and the run products well characterized, the K_{sp} value is more rigorously constrained than those from previous studies.

Sandino and Grambow [32], the only previous study of compreignacite solubility, measured the solubility of compreignacite by allowing metaschoepite to convert to compreignacite, and also by measuring the solubility of compreignacite directly. Their results produced $\lg K_{sp}$ values of (36.82 (±0.32)) and (39.16 (±0.31)) for the conversion and direct experiments, respectively. Neither experiment was conducted from supersaturation. Our $\lg K_{sp}$ value, obtained from supersaturation and undersaturation experiments, is in agreement with the conversion experiment value

from Sandino and Grambow [32]. The substitution of sodium for potassium in compreignacite appears to increase its solubility product by approximately 3.5 orders of magnitude, causing the equilibrium concentration of aqueous uranyl to increase by approximately 0.6 lg mol · kg^{-1} for the Na end-member relative to the K phase.

There have been no direct measurements of clarkeite solubility reported; however, Giammar and Hering [22,21] reported the formation of a clarkeite-like phase in two studies investigating the solubility of metaschoepite and the kinetics of soddyite dissolution. While these studies were not aimed at measuring the solubility of clarkeite, the authors were able to calculate some boundary values for its solubility product from their data. The lg K_{sp} values from the soddyite dissolution kinetics experiments and from the metaschoepite solubility experiments are (9.02) and (8.81) (no errors reported), respectively. Our clarkeite lg K_{sp} value (9.4 (−0.9/+0.6)) is consistent with both values reported by Giammar and Hering [22,21].

Figure 6 depicts calculated solubilities that demonstrate the dependence of the solubility of clarkeite on aqueous Na concentrations, and compares these solubilities to total aqueous uranium concentrations in equilibrium with metaschoepite. These calculations are conducted using our calculated K_{sp} values and stability constant values for the important uranyl aqueous complexes, listed in table 2. Metaschoepite solubility is independent of Na concentrations from (5 to 100) mM, while the solubility of clarkeite changes dramatically. For example at pH 6, clarkeite solubility decreases approximately three orders of magnitude when increasing the aqueous Na concentration from (5 to 100) mM. Clearly, the aqueous Na concentration exerts a strong control on uranium mobility in clarkeite-buffered systems.

As is suggested by the difference between our compreignacite and Na–compreignacite K_{sp} values, the identity of interlayer cations in uranyl phases can strongly influence the solubility behavior of the phases. This difference in solubility of these two phases is illustrated in figure 7, which depicts calculated total aqueous uranium concentrations in equilibrium with compreignacite and Na–compreignacite over a range of pH values. These calculations were conducted using our calculated K_{sp} values and stability constant values for the important uranyl aqueous complexes, listed in table 2. The substitution of Na for K in the compreignacite structure causes a decrease in equilibrium uranium concentration of approximately an order of magnitude over a wide range of pH conditions. In the environment, it is likely that mixed Na–K phases dominate relative to the pure end-member phases. It is possible that even a minor substitution of Na into compreignacite could have a large impact on the solubility of the mineral phase. In order to accurately predict the solubility of mixed phases, more data are needed that quantify the solubility of well-characterized mixed phases, thereby enabling the calculation of solid phase activity coefficients and the prediction of solubilities of the whole solid-solution range from compreignacite to Na–compreignacite. In general, virtually nothing is known about solid phase activity coefficients for any solid uranyl phases.

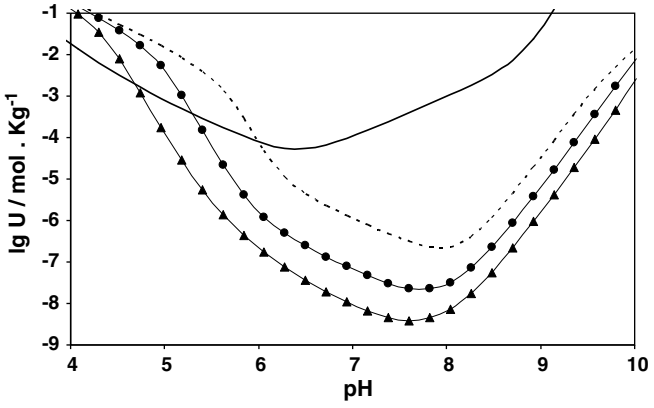

FIGURE 6. Plot of calculated solubilities U as lg(U/mol · kg^{-1}) against pH for clarkeite in (5, 25, and 100) mM Na^+, denoted by dashed, closed circle, and triangle curves, respectively, and metaschoepite, denoted by the solid curve.

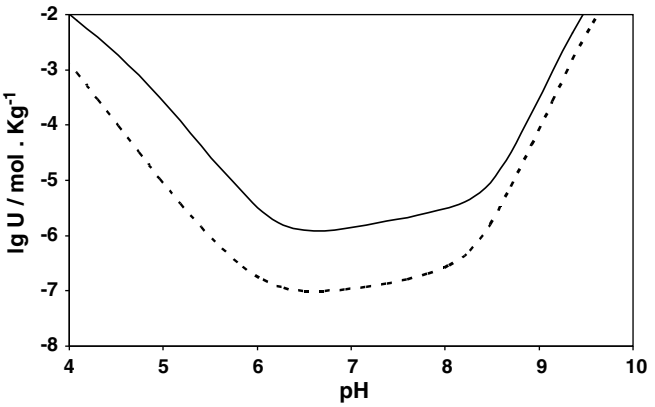

FIGURE 7. Plot of calculated solubilities U as lg(U/mol · kg^{-1}) against pH for compreignacite (solid curve) and Na–compreignacite (dashed curve) in 5 mM Na^+ and K^+.

3.3. Standard state Gibbs free energy, enthalpy, and entropy of formation

The standard-state Gibbs free energy of formation of each phase studied here was calculated from the equations shown in table 3. The literature values for $\Delta G^\circ_{f(UO_2^{2+})} = (-952.551 \pm 1.747)$ kJ mol^{-1}, $\Delta G^\circ_{f(Na^+)} = (-261.953 \pm 0.096)$ kJ · mol^{-1}, $\Delta G^\circ_{f(K^+)} = (-282.510 \pm 0.116)$ kJ · mol^{-1}, $\Delta G^\circ_{f(Ca^{2+})} = (-552.806 \pm 1.050)$ kJ · mol^{-1}, and $\Delta G^\circ_{f(H_2O)} = (-237.140 \pm 0.041)$ kJ · mol^{-1} were obtained from Cox *et al.* [36] and the standard state Gibbs free energy of reaction, ΔG°_r, was calculated from the corresponding K_{sp} value with the following equation:

$$\Delta G^\circ_r = -2.3026RT \cdot \lg K_{sp}, \quad (2)$$

TABLE 3

Mineral phase	Gibbs free energy of formation equations	$(\Delta G_f^\circ \pm 2\sigma)$/ (kJ · mol^{-1})	$(\Delta H_f^\circ \pm 2\sigma)$/ (kJ · mol^{-1})[a]	$(\Delta S_f^\circ \pm 2\sigma)$/ (J · mol^{-1} · K^{-1})
Metaschoepite	$\Delta G_f^\circ = 3 \cdot \Delta G^\circ_{f(H_2O)} + \Delta G^\circ_{f(UO_2^{2+})} - \Delta G_r^\circ$	−1632.2 (± 7.4)	−1791.0 (± 3.2)	−532.5 (± 8.1)
Becquerelite	$\Delta G_f^\circ = 18 \cdot \Delta G^\circ_{f(H_2O)} + 6 \cdot \Delta G^\circ_{f(UO_2^{2+})} + \Delta G^\circ_{f(Ca^{2+})} - \Delta G_r^\circ$	−10305.6 (± 26.5)	−11389.2 (± 13.5)	−3634.5 (± 29.7)
Compreignacite	$\Delta G_f^\circ = 17 \cdot \Delta G^\circ_{f(H_2O)} + 6 \cdot \Delta G^\circ_{f(UO_2^{2+})} + 2 \cdot \Delta G^\circ_{f(K^+)} - \Delta G_r^\circ$	−10107.3 (± 21.8)	No data available	
Sodium compreignacite	$\Delta G_f^\circ = 17 \cdot \Delta G^\circ_{f(H_2O)} + 6 \cdot \Delta G^\circ_{f(UO_2^{2+})} + 2 \cdot \Delta G^\circ_{f(Na^+)} - \Delta G_r^\circ$	−10045.6 (± 24.5)	−10936.4 (± 14.5)	−2987.6 (± 28.5)
Clarkeite	$\Delta G_f^\circ = 2 \cdot \Delta G^\circ_{f(H_2O)} + \Delta G^\circ_{f(UO_2^{2+})} + \Delta G^\circ_{f(Na^+)} - \Delta G_r^\circ$	−1635.1 (± 23.4)	−1724.7 (± 5.1)	−300.5 (± 23.9)

[a] All values from [18].

where R is the universal gas constant and T is absolute temperature. The 2σ errors associated with the ΔG_r° values are calculated by propagating the largest error associated with the respective $\lg K_{sp}$ values. We conduct these calculations for each solubility data point that was measured, and the average standard-state Gibbs free energy of formation for each mineral with its 2σ error is reported in table 3. The 2σ errors are calculated from propagating the errors associated with the ΔG_f° values of the mineral phase constituents and ΔG_r°.

Chen *et al.* [37] predicted the standard-state Gibbs free energy of formation of various uranyl minerals using an empirical approach that derives the molar contributions of the structural components to ΔG_f° and ΔH_f° from thermodynamic data of phases for which the crystal structures are known. The only mineral in our study for which Chen *et al.* made a prediction was becquerelite. Their value, −10324.7 kJ · mol^{-1}, is consistent with the calculated value based on our solubility measurements.

The standard-state entropy of formation of a solid phase, ΔS_f°, can be calculated from the standard-state Gibbs free energy and enthalpy of formation values:

$$\Delta G_f^\circ = \Delta H_f^\circ - T\Delta S_f^\circ, \quad (3)$$

where $\Delta G_f^\circ$is the standard-state Gibbs free energy of formation of the phase of interest, as determined from the solubility measurements, and ΔH_f° is the standard-state enthalpy of formation. Recently, Kubatko *et al.* [18] measured the enthalpy of formation for metaschoepite, becquerelite, sodium compreignacite, and clarkeite. Using equation (3), we calculated the standard-state entropy of formation for these minerals and these values are compiled in table 2.

4. Conclusions

The environmental fate of uranium under oxidizing conditions is controlled to a large extent by the formation of a variety of uranyl minerals, and the solubilities of these minerals strongly affects the release of uranium and other radionuclides that they incorporate. Therefore, it is crucial to augment the sparse thermodynamic dataset that exists for uranyl minerals in order to model the behavior of uranium in the environment. For example, standard-state Gibbs free energies, enthalpies, and entropies of formation for environmentally important uranyl minerals can be used to estimate mineral stabilities and solubilities under the elevated temperatures of a high-level nuclear waste repository setting. In this study, we measured the solubility of metaschoepite, becquerelite, compreignacite, Na–compreignacite, and clarkeite, using an experimental approach that enables a rigorous demonstration that equilibrium was attained during the experiments. The solubility measurements were used to calculate the standard-state Gibbs free energies of formation of the mineral phases, and together with the previously published standard state enthalpies of formation for metaschoepite, becquerelite, Na–compreignacite, and clarkeite, we calculated the standard-state entropies of formation of each of these solid phases. This study demonstrates the power of combining solubility and calorimetry measurements to produce reliable and internally-consistent thermodynamic data for uranyl minerals. The results of this and future similar studies of other environmentally relevant uranyl phases will enable predictions of uranyl mineral stabilities and solubilities under realistic environmental conditions.

Acknowledgements

Funding for this research was provided by a US Department of Energy, Office of Science and Technology and International (OST&I) grant under the Source Term Thrust program. Two journal reviews significantly improved the presentation of this manuscript.

Appendix A. Supplementary data

Supplementary data associated with this article can be found, in the online version, at doi:10.1016/j.jct.2008.02.006.

References

[1] R.J. Finch, T. Murakami, in: P.C. Burns, R.J. Finch (Eds.), Systematics and Paragenesis of Uranium Minerals, Mineralogical Society of America, Washington, DC, 1999, pp. 91–180.
[2] P.C. Burns, Can. Mineral. 43 (2005) 1839–1894.
[3] M. Schindler, F.C. Hawthorne, Can. Mineral. 42 (2004) 1601–1627.
[4] M. Schindler, F.C. Hawthorne, P.C. Burns, P.A. Maurice, Can. Mineral. 44 (2006) 1207–1225.
[5] R.J. Finch, R.C. Ewing, J. Nucl. Mater. 190 (1992) 133–156.

[6] C. Frondel, Am. Mineral. 41 (1956) 539.
[7] R.J. Finch, E.C. Buck, P.A. Finn, J.K. Bates, Mater. Res. Soc. Symp. Proc. 556 (1999) 431–438.
[8] D.J. Wronkiewicz, J.K. Bates, T.J. Gerding, E. Veleckis, B.S. Tani, J. Nucl. Mater. 190 (1992) 107–127.
[9] D.J. Wronkiewicz, J.K. Bates, S.F. Wolf, E.C. Buck, J. Nucl. Mater. 238 (1996) 78–95.
[10] R.J. Finch, M.L. Miller, R.C. Ewing, Radiochim. Acta 58-9 (1992) 433–443.
[11] E.C. Pearcy, J.D. Prikryl, W.M. Murphy, B.W. Leslie, Appl. Geochem. 9 (1994) 713–732.
[12] P.C. Burns, P.C. Ewing, M.L. Miller, J. Nucl. Mater. 245 (1997) 1–9.
[13] P.C. Burns, K.M. Deely, S. Skanthakumar, Radiochim. Acta 92 (2004) 151–159.
[14] M. Douglas, S.B. Clark, J.I. Friese, B.W. Arey, E.C. Buck, B.D. Hanson, S. Utsunomiya, R.C. Ewing, Radiochim. Acta 93 (2005) 265–272.
[15] M. Douglas, S.B. Clark, J.I. Friese, B.W. Arey, E.C. Buck, B.D. Hanson, Environ. Sci. Technol. 39 (2005) 4117–4124.
[16] A.L. Klingensmith, K.M. Deely, W.S. Kinman, V. Kelly, P.C. Burns, Am. Mineral. 92 (2007) 662–669.
[17] D. Gorman-Lewis, P.C. Burns, J.B. Fein, J. Chem. Thermodyn. 40 (2008) 335–352.
[18] K.-A. Kubatko, K. Helean, A. Navrotsky, P.C. Burns, Am. Mineral. 91 (2006) 658–666.
[19] J. Cjeka, in: P.C. Burns, R.J. Finch (Eds.), Infrared Spectroscopic and Thermal Analysis of the Uranyl Minerals, Mineralogical Society of America, Washington, DC, 1999, pp. 521–622.
[20] J.A. Illingworth, Biochem. J. 195 (1981) 259–262.
[21] D.E. Giammar, J.G. Hering, Environ. Sci. Technol. 38 (2004) 171–179.
[22] D.E. Giammar, J.G. Hering, Geochim. Cosmochim. Acta 66 (2002) 3235–3245.
[23] D.J. Gorman-Lewis, L. Mazeina, B. Fein Jeremy, J. Szymanowski, P.C. Burns, A. Navrotsky, J. Chem. Thermodyn. 39 (2007) 568–575.
[24] P.C. Burns, in: P.C. Burns, R.J. Finch (Eds.), The Crystal Chemistry of Uranium, Mineralogical Society of America, Washington, DC, 1999, pp. 23–90.
[25] H.C. Helgeson, D.H. Kirkham, G.C. Flowers, Am. J. Sci. 281 (1981) 1249–1516.
[26] D. Langmuir, Aqueous Environmental Geochemistry, Prentice Hall Inc., Englewood Cliffs, NJ, 1997.
[27] J. Bruno, A. Sandino, Mater. Res. Soc. Symp. Proc. 127 (1989) 871–878.
[28] A. Sandino, J. Bruno, Geochim. Cosmochim. Acta 56 (1992) 4135–4145.
[29] U. Kramer-Schnabel, H. Bischoff, R.H. Xi, G. Marx, Radiochim. Acta 56 (1992) 183–188.
[30] G. Meinrath, T. Kimura, Inorg. Chim. Acta 204 (1993) 79–85.
[31] G. Meinrath, Y. Kato, T. Kimura, Z. Yoshida, Radiochim. Acta 75 (1996) 159–167.
[32] M.C.A. Sandino, B. Grambow, Radiochim. Acta 66–67 (1994) 37–43.
[33] R. Vochten, L. Van Haverbeke, Miner. Petrol. 43 (1990) 65–72.
[34] B.D. Rai, A.R. Felmy, N.J. Hess, V.L. LeGore, D.E. McCready, Radiochim. Acta 90 (2002) 495–503.
[35] I. Casas, J. Bruno, E. Cera, R.J. Finch, R.C. Ewing, Geochim. Cosmochim. Acta 61 (1997) 3879–3884.
[36] J.D. Cox, D.D. Wagman, V.A. Medvedev, CODATA Key Values for Thermodynamics, Hemisphere Publishing Corporation, New York, 1989.
[37] F.R. Chen, R.C. Ewing, S.B. Clark, Am. Mineral. 84 (1999) 650–664.
[38] R. Guillaumont, T. Fanghanel, J. Fuger, I. Grenthe, V. Neck, D. Palmer, M. Rand, Update on the Chemical Thermodynamics of Uranium, Neptunium, and Plutonium, second ed., Elsevier, Amsterdam, 2003.
[39] A.E. Martell, NIST Critically Selected Stability Constants of Metal Complexes, Database, 6.0 for Windows, U.S. Department of Commerce, Technology Administration, National Institute of Standards and Technology, Gaithersburg, MD, 2001.

JCT 07-371